

5. P. Rich, personal communication.
6. A. E. Newsome, *Aust. J. Zool.* **13**, 735 (1965).
7. G. B. Sharman, H. J. Frith, J. H. Calaby, *CSIRO Wildl. Res.* **9**, 20 (1964).
8. D. R. Horton and J. Samuel, *Aust. J. Zool.*, in press.
9. P. Crabb, personal communication.
10. See also D. R. Horton, *Artefact* **1** (No. 3), 129 (1976).
11. D. R. Horton, *Aust. Inst. Aboriginal Stud. Newsl.* **9**, 27 (1978).
12. For the method see R. Gillespie and R. B. Temple, *Radiocarbon* **15**, 566 (1973).
13. R. M. Jones, *Archaeol. Phys. Anthropol. Oceania* **3**, 186 (1968).
14. The work at Lancefield has been supported by grants from the University of Sydney, the Australian Institute of Aboriginal Studies, the National Museum of Victoria, and the Department of Mines. This report was edited by R.V.S.W.

6 December 1977; revised 6 March 1978

Atomic Hydrogen on Mars: Measurements at Solar Minimum

Abstract. *The Copernicus Orbiting Astronomical Observatory was used to obtain measurements of Mars Lyman- α (1215.671- \AA) emission at the solar minimum, which has resulted in the first information on atomic hydrogen concentrations in the upper atmosphere of Mars at the solar minimum. The Copernicus measurements, coupled with the Viking in situ measurements of the temperature ($170^\circ \pm 30^\circ\text{K}$) of the upper atmosphere of Mars, indicate that the atomic hydrogen number density at the exobase of Mars (250 kilometers) is about 60 times greater than that deduced from Mariner 6 and 7 Lyman- α measurements obtained during a period of high solar activity. The Copernicus results are consistent with Hunten's hypothesis of the diffusion-limited escape of atomic hydrogen from Mars.*

A bright Lyman- α (1215.671- \AA) day-glow, arising from the resonant scattering of solar Lyman- α photons by atomic hydrogen (H), appears to be a regular feature of planetary exospheres. Rockets, satellites, and planetary probes have measured Lyman- α emission emanating from the terrestrial exosphere and the geocorona, as well as from the hydrogen coronae of Mars (measured by Mariner 6, 7, and 9), Venus (Mariner 5 and 10), Mercury (Mariner 10), and Jupiter (Pio-

neer 10 and 11). A comprehensive review of the hydrogen coronae of the terrestrial planets has recently appeared (1).

The first measurements of Mars Lyman- α emission were obtained in July and August 1969 with the ultraviolet spectrometers aboard the Mariner 6 and 7 flybys during a period of high solar activity (2, 3). A similar ultraviolet spectrometer aboard the Mariner 9 orbiter obtained Mars Lyman- α measurements

between November 1971 and February 1972, also during a period of high solar activity (4, 5). Interpretation of the Mariner Mars Lyman- α emission measurements with a spherical radiative transfer model has led to our present understanding of both the H distribution in the martian corona and the escape of H from Mars (3, 5). Knowledge of the exospheric distribution and escape of H (a photolytic product of H_2O), and of how the distribution and escape of H vary with the level of solar activity, is important in assessing the evolution of H_2O over the history of Mars (6).

We report here on the first measurements of Mars Lyman- α emission obtained during a period of low solar activity. In addition, the measurements obtained with the Copernicus Orbiting Astronomical Observatory (OAO-3) are the first measurements of Mars Lyman- α emission obtained from the vicinity of Earth. We will discuss the characteristics of the Mars hydrogen corona, deduced from our analysis of these measurements, coupled with the recent Viking in situ measurements of the upper atmospheric temperature of Mars, and will compare them with the Mariner 6 and 7 Lyman- α measurements.

Copernicus was launched into a 750-km circular orbit in August 1972. The Princeton Experiment Package (PEP) on Copernicus consists of a 32-inch (80-cm) Cassegrain telescope with a Paschen-Runge spectrometer, which utilizes a concave grating to focus the spectrum on a 1-m Rowland circle. Two movable carriages, each equipped with two photomultiplier tubes, scan the spectrum. For the Mars measurements, we used the U1 photomultiplier tube with a band-pass width of 0.04 \AA , centered at the H Lyman- α line at 1215.671 \AA . The spectrometer entrance slit was placed on the centroid of light of the visible disk of Mars. The Copernicus entrance slit is 39 arc sec long by 0.3 arc sec wide. In September 1975, Mars was about 9 arc sec in diameter. The spectrometer scan is placed at the blue end of the line and is moved every 14 seconds to a new position in 0.02- \AA intervals across the line. The complete scan from about 1215.5 to 1215.8 \AA takes about 8 minutes.

The Copernicus measurement procedure consisted of one orbit ON Mars, followed by one orbit OFF Mars (about 60 arc sec off the Mars disk). The ON-OFF measurement procedure continued for about 11 orbits on 6 to 8 September 1975, yielding a total of about 49 scans of the geocorona and Mars Lyman- α emission spectra.

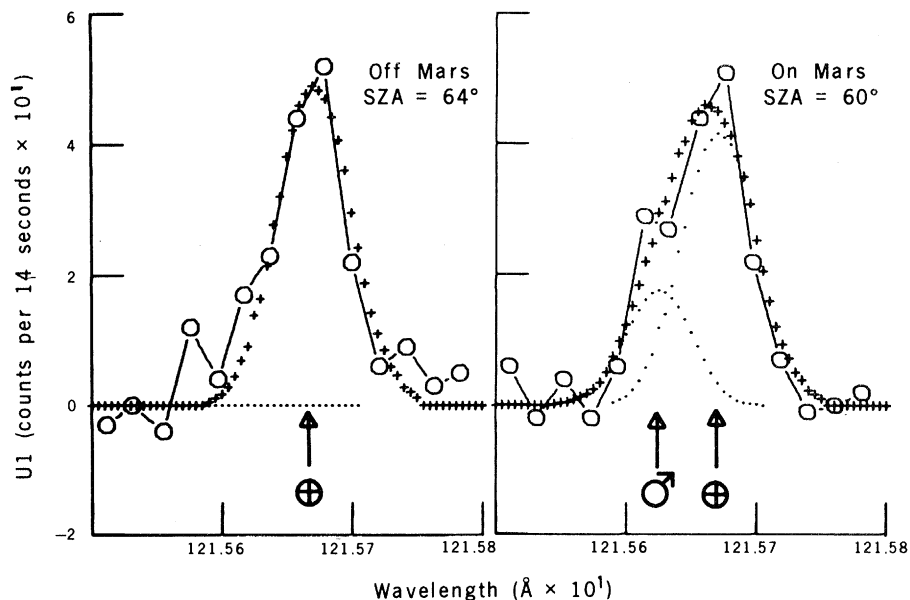


Fig. 1 (left). Copernicus spectrum of geocoronal Lyman- α radiation (OFF Mars) for SZA = 64° . The vertical arrow indicates the Lyman- α line center. The circles are the Copernicus measurements, and the pluses are derived from a least-squares fit (see text). Fig. 2 (right). Copernicus spectrum of geocoronal and Mars Lyman- α radiation (ON Mars) for SZA = 60° . The vertical arrows indicate the Mars and geocoronal Lyman- α line centers. The circles are the Copernicus measurements; the pluses are derived from a least-squares fit and are the sum of the two individual profiles of the geocorona and Mars Lyman- α spectrum indicated by the small dots.

The spectrum of geocoronal Lyman- α radiation for a typical OFF orbit is shown in Fig. 1. The pluses are derived from a least-mean-squares analysis, in which the height of an assumed geocoronal profile shape is allowed to vary until the root-mean-square residual between the measurements and the profile is minimized. In this way, the entire measurement profile is included in the data analysis. The solar zenith angle (SZA) is defined as the angle subtended by the satellite's local zenith and the sun.

The spectrum of the geocoronal and Mars Lyman- α dayglow for a typical ON orbit (at about the same SZA as that for the OFF orbit) is shown in Fig. 2. The pluses are the sum of the assumed geocoronal and Mars profile shapes, the heights of which are allowed to vary independently until the root-mean-square residual between the measurements (circles) and the sum of the profiles (pluses) is minimized. In this way, the entire measurement spectrum is used to separate the geocoronal and Mars signals. The Mars Lyman- α signal is Doppler-shifted 0.04 Å to the blue, since Mars was approaching Earth at about 40 km/sec, and is easily identified in the blue wing of the stronger geocoronal signal.

The individual Copernicus geocorona Lyman- α measurements, as a function of SZA, are shown in Fig. 3, along with the linearly averaged value of the measurements, grouped around certain intervals of the SZA. The vertical bars represent ± 1 sigma error of the mean, and the horizontal error bars are the SZA interval over which the measurements were averaged.

The geocoronal Lyman- α measurements obtained from both the ON (after separating the Mars signal) and the OFF orbits were made over a wide range of values of SZA. The solid curve in Fig. 3 is the theoretical curve that best fits the data and was generated with a geocoronal Lyman- α resonance scattering radiative transfer model (3, 7). The model includes the theoretical calculation of the density distribution of H and the resonance scattering of solar Lyman- α photons by the hydrogen atoms in a spherically symmetric isothermal geocorona. The exospheric temperature (T_e) and the H number density at the critical level or exobase (500 km) (n_c) were 800°K and $2 \times 10^5 \text{ cm}^{-3}$, respectively.

Conversion of Copernicus measurements to a hydrogen column abundance (density) on Mars does not depend on explicit knowledge of either the solar flux or the calibration of the Copernicus instrument. The geocoronal hydrogen

column density may be uniquely determined from an analysis of the variation of the Lyman- α intensity measured by Copernicus for different values of SZA about the orbit. It is the shape and not the absolute value of the Lyman- α intensity about the orbit that determines the hydrogen column density. The hydrogen column density on Mars may then be inferred directly from the geocoronal measurements because the measurements were made simultaneously with the same instrument. This direct inference eliminates the necessity for absolute calibration of the signal.

Once the column abundance is determined for both Mars and Earth, the Copernicus measurements may be related to absolute Lyman- α intensities (in kilo-Rayleighs), by assigning a solar flux based on solar activity ($1 \text{ kR} = 10^9 \text{ photon cm}^{-2} \text{ sec}^{-1}$) (8). This calibration of the data is not necessary for the determination of hydrogen on Mars from the Copernicus measurements but we have carried it out in order to be able to compare the Copernicus Lyman- α measurements with other planetary Lyman- α measurements. The right-hand ordinate in Figs. 3 and 4 gives the intensity for a value of the solar flux equal to $\pi F_0 = 2.4 \times 10^{11} \text{ photon cm}^{-2} \text{ sec}^{-1} \text{ Å}^{-1}$ (8).

The Copernicus Mars measurements (Fig. 4) do not exhibit any systematic variation around the orbit, an indication

that the data reduction techniques successfully separate the Mars signals from the ON orbit spectra. The average Mars signal of 14.2 counts per 14 seconds has an uncertainty of about 25 percent or about ± 3.5 counts per 14 seconds. This uncertainty includes uncertainties introduced by model parameters, measurement errors, and possible day-to-day variations in solar Lyman- α emission. Analysis of the variation of Copernicus measurements at SZA = 40° indicates that over the measurement period the variability of solar Lyman- α was about ± 12 percent. The average Mars signal of 14.2 ± 3.5 counts per 14 seconds corresponds to a Copernicus slit intensity of $3.6 \pm 0.8 \text{ kR}$. Subtracting the interplanetary Lyman- α background results in a Copernicus slit intensity of $3.3 \pm 0.8 \text{ kR}$.

An interplanetary Lyman- α background of about 0.3 kR accounts for the observed difference between the model and the measurements at large values of SZA. The background value is comparable with other interplanetary Lyman- α background measurements (9).

The same radiative transfer scattering model used to analyze the Mariner Mars Lyman- α measurements (7) was used in the analysis of the Copernicus geocoronal Lyman- α measurements and in the interpretation of the Copernicus Mars Lyman- α measurements. The scattering

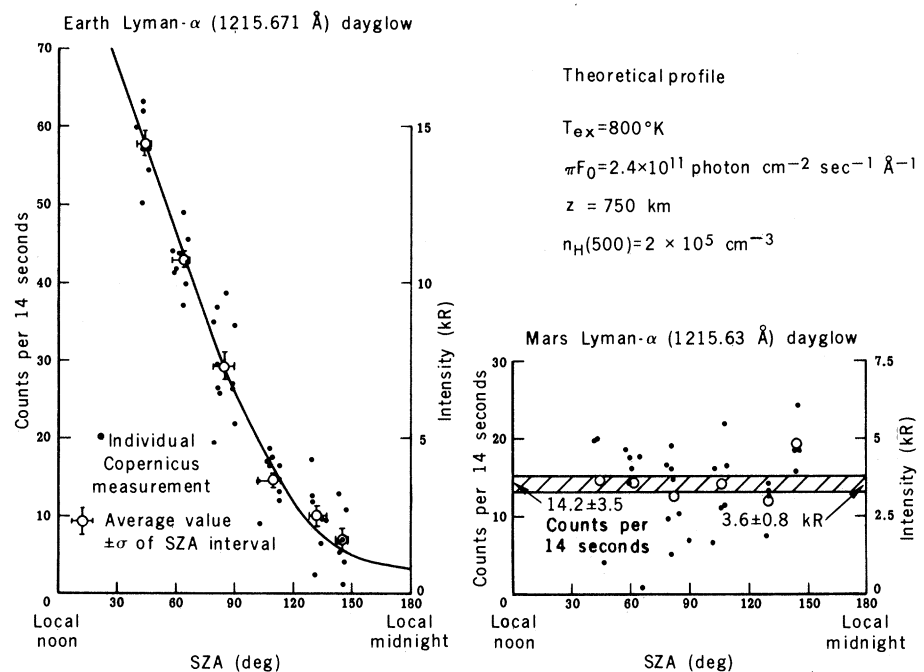


Fig. 3 (left). The variation of geocoronal Lyman- α radiation about the orbital plane. The individual Copernicus measurements are shown as dots, which are averaged into intervals of the SZA, shown as circles. The solid line is a theoretical profile (see text). Fig. 4 (right). Mars Lyman- α radiation as measured about the orbital plane. The individual Copernicus measurements are shown as dots, which are averaged into intervals of the SZA, shown as circles. The diagonal-lined area is ± 1 sigma error of the mean. The average Copernicus Mars Lyman- α slit intensity is $3.6 \pm 0.8 \text{ kR}$.

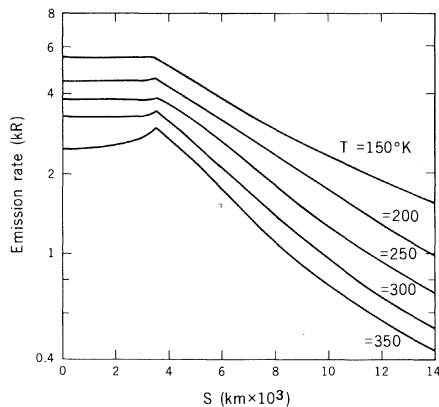


Fig. 5. Theoretical Mars Lyman- α emission rates. Intensities are plotted in kilorayleighs as a function of distance S along the Copernicus slit for five exospheric temperatures, T_c , where n_c for each model is calculated for $\phi_c = 1.4 \times 10^8 \text{ cm}^{-2} \text{ sec}^{-1}$.

model includes effects due to the presence of pure absorbers in the scattering region— O_2 for Earth and CO_2 for Mars. The lower boundary of this region is taken as the level where pure absorption becomes important, 100 km for Earth and 80 km for Mars.

In the absence of photochemical or other sources or sinks of hydrogen within the scattering region, the H density distribution, $n(z)$ where z is the distance above the surface (in kilometers), may be characterized by the following parameters at the critical level or exobase: T_c , n_c , and the flux of escaping hydrogen atoms, ϕ_c . For Earth, the effect of photochemical sources of H between 100 and 150 km on the Lyman- α signal is small and hence was neglected. For Mars, photochemical sources of H produce significant changes in $n(z)$ between 80 and 150 km. We approximated these changes in the Mars model by allowing $n(z)$ to decrease exponentially from 80 to 150 km, with $n(80) = 2 \times 10^6 \text{ cm}^{-3}$ for $T_c = 350^\circ\text{K}$, and $n(80) = 1 \times 10^7 \text{ cm}^{-3}$ for all other values of T_c (5). The density was matched to its diffusion-limited value at 150 km.

Analysis of the Mariner 6 and 7 ultraviolet spectrometer Lyman- α measurements, made during a period of high solar activity, indicated that $T_c = 350^\circ\text{K}$ and $n_c = 2.5 \times 10^4$ (3). The Copernicus Lyman- α measurements were made during a period of low solar activity and hence during a period of lower Mars exospheric temperature. The value of T_c deduced from the Mariner 6 and 7 measurements may be taken as an upper limit in our Copernicus analysis. The values for T_c and n_c deduced from the Mariner 6 and 7 measurements yield $\phi_c = 1.4 \times 10^8 \text{ cm}^{-2} \text{ sec}^{-1}$, based on the classical Jeans

theory of escape (10). The Mariner-deduced value of ϕ_c appears to be applicable to our Copernicus measurements. On the basis of theoretical considerations, Hunten has suggested that ϕ_c is not dependent on T_c but is diffusion-limited and controlled by the total mixing ratio of hydrogen species in the lower atmosphere (11).

To test the diffusion-limited constant escape flux hypothesis, we calculated altitude profiles for several values of T_c , with n_c chosen so that $\phi_c = 1.4 \times 10^8 \text{ cm}^{-2} \text{ sec}^{-1}$. These emission profiles are shown in Fig. 5 for values of $T_c = 150^\circ, 200^\circ, 250^\circ, 300^\circ,$ and 350°K . At all altitudes the emission rate increases for decreasing T_c . This result is a consequence of increasing n_c , with a decreasing T_c in order to keep ϕ_c constant.

The Copernicus measurements represent the sum of both the disk and limb components of Mars Lyman- α emission, since the entrance slit of the instrument covers a field of view of 28,000 km by 200 km centered on the visible disk of Mars. In order to compare the Copernicus measurements with the theoretical model calculations, the emission rate profiles must be averaged over the slit area to determine the slit-averaged intensity. The slit-averaged intensity, corresponding to the emission rate profiles given in Fig. 5, are shown in Fig. 6, as a solid line plotted as a function of T_c . The dashed line shows the variation of n_c with T_c , assuming $\phi_c = 1.4 \times 10^8 \text{ cm}^{-2} \text{ sec}^{-1}$.

Unlike the Mariner Lyman- α measurements, there is no detailed altitude information in the Copernicus measurements, and therefore a unique set of coupled values of T_c and n_c to fit the Copernicus measurements does not exist. A value of n_c may be found for each value of T_c that will yield agreement with the measurements. For example, if $T_c = 350^\circ\text{K}$, then the value of n_c is more than three times the 1969 value of n_c deduced from Mariner 6 and 7 measurements (see data points A, B, and C in Fig. 6; point A corresponds to the intensity based on the use of Mariner 6 and 7 deduced values of T_c and n_c ; B corresponds to the intensity for twice the Mariner value of n_c ; and C corresponds to the intensity for three times the Mariner value of n_c).

In our pre-Viking analysis of the Copernicus measurements, we assumed that $T_c = 250^\circ\text{K}$ and that the escape of H was diffusion-limited (and used the H flux deduced from Mariner 6 and 7). For these assumptions, we found more than a fourfold increase in n_c compared to the Mariner 6 and 7 results (12). The recent

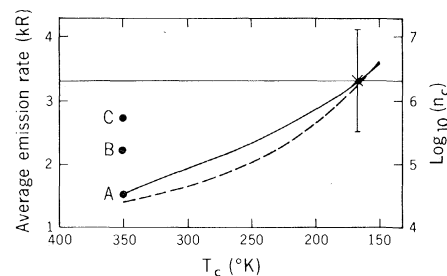


Fig. 6. Model results. The horizontal line at 3.3 kR indicates the Copernicus Mars Lyman- α intensity with error bars as shown. Points A, B, and C represent theoretical average emission rates with $n_c = 1, 2,$ and $3 n_c$ (350°K) and $\phi_c = 1, 2,$ and $3 \phi_c$ (350°K), where n_c (350°K) = $2.5 \times 10^4 \text{ cm}^{-3}$ and ϕ_c (350°K) = $1.4 \times 10^8 \text{ cm}^{-2} \text{ sec}^{-1}$. The solid curve is the theoretical average emission rate plotted as a function of T_c with n_c chosen such that $\phi_c = 1.4 \times 10^8 \text{ cm}^{-2} \text{ sec}^{-1}$, with $\log_{10} n_c$ represented by the dashed curve. The cross indicates the estimated value of n_c based on the theoretical calculations of the average emission rate.

Viking in situ measurements, which indicated a much lower upper atmospheric temperature than previously believed, $170^\circ \pm 30^\circ\text{K}$ (13), have led to a reanalysis of the Copernicus measurements. Using Fig. 6 and the Viking-measured upper atmospheric temperature of $170^\circ \pm 30^\circ\text{K}$, we now find a value of $n_c = 60$ times the Mariner 6 and 7 value of n_c . This large buildup of H in the upper atmosphere of Mars at solar minimum deduced from the Copernicus measurements is a direct consequence of the lower H effusion velocity associated with the lower exospheric temperature at solar minimum. The hypothesis of diffusion-limited escape flux requires that the product of n_c and the effusion velocity remains constant, independent of solar activity (11). The Copernicus measurements of Lyman- α intensity, coupled with the Viking measurements of upper atmospheric temperature, are consistent with the concept of diffusion-limited escape flux.

It has been suggested that the nonthermal escape of atomic oxygen (O) controls the thermal escape of H since the escape of O regulates the production of molecular hydrogen, which in turn controls the production and hence the escape of H via the ionospheric reaction of the carbon dioxide ion with molecular hydrogen (14). Since the nonthermal escape of O is controlled by ionospheric processes (14) and since Viking measurements (13) indicate a Mars ionosphere comparable to that measured by Mariner 6, 7, and 9, the escape of O during the Copernicus measurement period was probably comparable to that of the Mari-

ner measurements in 1969 and 1971. This implies no significant change in the escape of H due to nonthermal mechanisms.

JOEL S. LEVINE

DAVID S. MCDUGAL

NASA Langley Research Center,
Hampton, Virginia 23665

DONALD E. ANDERSON, JR.

E. O. Hulburt Center for Space
Research, Naval Research Laboratory,
Washington, D.C. 20375

EDWIN S. BARKER

Princeton University Observatory,
Princeton, New Jersey 08540

References and Notes

1. D. M. Hunten and T. M. Donahue, *Annu. Rev. Earth Planet. Sci.* **4**, 265 (1976).
2. C. A. Barth, W. G. Fastie, C. W. Hord, J. B. Pearce, K. K. Kelly, A. I. Stewart, G. E. Thomas, G. P. Anderson, O. F. Raper, *Science* **165**, 1004 (1969); C. A. Barth, C. W. Hord, J. B. Pearce, K. K. Kelly, G. P. Anderson, A. I. Stewart, *J. Geophys. Res.* **76**, 2213 (1971).
3. D. E. Anderson, Jr., and C. W. Hord, *J. Geophys. Res.* **76**, 6666 (1971).
4. C. A. Barth, C. W. Hord, A. I. Stewart, A. L. Lane, *Science* **175**, 309 (1972); C. A. Barth, A. I. Stewart, C. W. Hord, A. L. Lane, *Icarus* **17**, 457 (1972); A. I. Stewart, C. A. Barth, C. W. Hord, A. L. Lane, *ibid.*, p. 469.
5. D. J. Strickland and D. E. Anderson, Jr., *J. Geophys. Res.* **78**, 6491 (1973); D. E. Anderson, Jr., *ibid.* **79**, 1513 (1974); thesis, University of Colorado (1973).
6. J. S. Levine, *Icarus* **28**, 165 (1976); in *Proceedings of the Colloquium on Water in Planetary Regoliths* (U.S. Army Cold Regions Research and Engineering Laboratory, Hanover, N.H., 1977), p. 34; in *Comparative Planetology*, C. Ponnampuram, Ed. (Academic Press, New York, in press).
7. D. E. Anderson, Jr., and C. W. Hord, *Planet. Space Sci.* **25**, 563 (1977).
8. G. E. Thomas and D. E. Anderson, Jr., *ibid.* **24**, 303 (1976).
9. G. E. Thomas and R. F. Krassa, *Astron. Astrophys.* **11**, 218 (1971).
10. J. H. Jeans, *The Dynamical Theory of Gases* (Cambridge Univ. Press, Cambridge, 1916).
11. D. M. Hunten, *J. Atmos. Sci.* **30**, 1481 (1973).
12. D. S. McDougal, J. S. Levine, E. S. Barker, D. E. Anderson, Jr., *Bull. Am. Astron. Soc.* **8**, 481 (1976); J. S. Levine, D. S. McDougal, E. S. Barker, D. E. Anderson, Jr., *EOS Trans. Am. Geophys. Union* **57**, 293 (1976); D. E. Anderson, Jr., D. S. McDougal, J. S. Levine, E. S. Barker, *ibid.*, p. 293.
13. A. O. Nier, W. B. Hanson, A. Seiff, M. B. McElroy, N. W. Spencer, R. J. Duckett, T. C. D. Knight, W. S. Cook, *Science* **193**, 786 (1976); M. B. McElroy, T. Y. Kong, Y. L. Yung, A. O. Nier, *ibid.* **194**, 1295 (1976).
14. M. B. McElroy, *ibid.* **175**, 443 (1972); ——— and T. M. Donahue, *ibid.* **177**, 986 (1972); S. C. Liu and T. M. Donahue, *Icarus* **28**, 231 (1976).
15. J.S.L. and D.S.M. acknowledge their selection as guest investigators with the Princeton University telescope on the Copernicus satellite, which is sponsored and operated by National Aeronautics and Space Administration. We acknowledge the hospitality provided us by Dr. L. Spitzer during our visits to Princeton University Observatory and the assistance provided by Drs. Theodore P. Snow and Donald G. York of Princeton during the course of this investigation. We also thank Marvin R. Libson, Integrated Services, Inc., Hampton, Va., for helpful discussions.

31 May 1977; revised 28 December 1977

Winter Rain and Summer Ozone: A Predictive Relationship

Abstract. *Insights from dendrochronology have provided a new seasonal predictor for air pollution meteorology. In the San Francisco Bay Area summer ozone excesses over the federal ozone standard are correlated (correlation coefficient $r = .87$) with precipitation for the two preceding winters, a factor related to tree-ring width in a precipitation-stressed climate. The hypothesis that reactive hydrocarbon emissions from vegetative biomass affects these ozone excesses was supported by a similar correlation between summer hydrocarbon average maximums and the two-winter precipitation factor, reaching $r = .88$ at suburban stations. A weak tendency for hot summers to follow wet winters (in 16 years of California data) explains only a minor part of the ozone-rain relationship in multiple correlations.*

In assessing long-term trends for boundary-layer ozone in the San Francisco air basin, a linear decrease of 5 percent per year was found to fit the basic data [days on which ozone levels exceeded the federal standard of 0.08 part per million (ppm) for 1 hour] from 1965 through 1977, but the trace was very noisy, with year-to-year variations frequently exceeding 30 percent (see Fig. 1).

A reporter's counterintuitive question led to an explanation of most of this variability. The question, "Did the drought have anything to do with our clean air in 1977?" led to an examination of rainfall data in conjunction with ozone data. The rare summer rains in California are associated with good vertical mixing and gen-

erally clean air. Thus a negative relationship between precipitation and ozone has been generally assumed to exist. The discovery of a strong positive relationship between winter rain and summer ozone, reinforced by a similar positive relationship between winter rain and summer hydrocarbon levels, has provided a seasonal predictor of summer ozone excesses.

Fortunately an excellent data base has been developed for the air basin in 16 years of continuous monitoring by the Bay Area Air Pollution Control District (BAAPCD). All data obtained before June 1975 have been adjusted in accord with the California Air Resources Board (CARB) calibration procedures of that date, and thus are comparable with later

data. The monitoring network expanded from six urban stations in 1962 to 25 stations extending far into exurbia by 1975. The increase of ozone excesses in the period 1967 to 1969 was associated with the extension of the network to its first site (Livermore) away from urban centers, but in the downwind urban plume. Other new stations on the urban margins have added to the excess-day total in the air basin, but new stations in urban centers have had very little effect on observed ozone totals. The fact that excess days have decreased more than 60 percent in 12 years despite a fourfold amplification of the station network attests to both the reality of the decrease and the relative smoothness of the horizontal gradient of ozone. Precipitation is measured at about 70 stations in and near the San Francisco air basin, and monthly and annual totals are reported by the Environmental Data Service of the National Oceanic and Atmospheric Administration in *Climatological Data, Annual Summaries for California*. These data include an average for the Central Coast Drainage Basin, which is somewhat offset to the south of the San Francisco air basin, but encompasses the area where most ozone excesses occur.

Initial examination of the rainfall and ozone data sets (Fig. 1) and various exploratory correlations (Table 1) showed winter rainfall to be a strong leading indicator of summer ozone excesses. This counterintuitive relationship was then examined in detail, to seek out the strongest operational predictors and to examine the hypotheses that might explain it. These two goals were pursued concurrently, since predictors were developed through hypothesis testing.

Two major hypotheses were investigated. In hypothesis A, a purely meteorological relationship or forcing function, wet winters are precursors of hot stagnant summers that are conducive to photochemical oxidant formation. A corollary of A might include gradual rather than sudden advection of stratospheric ozone associated with strong subsidence during hot summers. In hypothesis B vegetative biomass increases with increased rainfall, leading to an increase of natural hydrocarbon emissions from this biomass.

Major features of the exploration of the ozone-rain relationship are summarized in Table 1. The independent variable of precipitation was first taken as an annual total from July through June in the California rainy season format, then narrowed to November through March in a non-ozone season format, and final-